

Numerical modeling of DNA-chip hybridization with chaotic advection

Florence Raynal, Aurélien Beuf, and Philippe Carrière

Citation: [Biomicrofluidics](#) 7, 034107 (2013); doi: 10.1063/1.4809518

View online: <http://dx.doi.org/10.1063/1.4809518>

View Table of Contents: <http://bmf.aip.org/resource/1/BIOMGB/v7/i3>

Published by the [American Institute of Physics](#).

Additional information on Biomicrofluidics

Journal Homepage: <http://bmf.aip.org/>

Journal Information: http://bmf.aip.org/about/about_the_journal

Top downloads: http://bmf.aip.org/features/most_downloaded

Information for Authors: <http://bmf.aip.org/authors>

ADVERTISEMENT



Goodfellow
metals • ceramics • polymers • composites
70,000 products
450 different materials
small quantities *fast*

www.goodfellowusa.com

Numerical modeling of DNA-chip hybridization with chaotic advection

Florence Raynal, Aurélien Beuf, and Philippe Carrière

LMFA, CNRS–Université de Lyon, École Centrale de Lyon–Université Lyon 1–INSA Lyon,
 École Centrale de Lyon, 36 avenue Guy de Collongue, 69134 Écully cédex, France

(Received 7 April 2013; accepted 21 May 2013; published online 3 June 2013)

We present numerical simulations of DNA-chip hybridization, both in the “static” and “dynamical” cases. In the static case, transport of free targets is limited by molecular diffusion; in the dynamical case, an efficient mixing is achieved by chaotic advection, with a periodic protocol using pumps in a rectangular chamber. This protocol has been shown to achieve rapid and homogeneous mixing. We suppose in our model that all free targets are identical; the chip has different spots on which the probes are fixed, also all identical, and complementary to the targets. The reaction model is an infinite sink potential of width d_h , i.e., a target is captured as soon as it comes close enough to a probe, at a distance lower than d_h . Our results prove that mixing with chaotic advection enables much more rapid hybridization than the static case. We show and explain why the potential width d_h does not play an important role in the final results, and we discuss the role of molecular diffusion. We also recover realistic reaction rates in the static case. © 2013 AIP Publishing LLC.
[\[http://dx.doi.org/10.1063/1.4809518\]](http://dx.doi.org/10.1063/1.4809518)

I. INTRODUCTION

In any system that requires chemical reactions, an efficient mixing is needed in order to homogenize the solutions, so as to favor the meeting of reactants. In microfluidics, however, the Reynolds number of flows at the microscale is small, generally of the order of unity or smaller, so that Stokes flows should be commonly expected.¹ It is well-known that chaotic advection is the best way to mix efficiently in laminar flows,^{2–8} all the more for microfluidic flows. We deal here with microfluidic systems where the height is small (typically 25–50 μm) and the length and width are “large,” of the order of the centimeter, such as those used for DNA-chip technology.

DNA chip technology is aimed to detect rapidly specific DNA sequences. A DNA chip is composed of a solid surface (such as glass) onto which arrays of biological probes (single stranded DNA) are fixed (Figure 1(a)).⁹ Each probe is made of 10 to 60 predetermined oligonucleotides. The working principle of DNA micro-arrays is the so-called *hybridization* phenomenon: when the chip is exposed to single-stranded DNA samples (*targets*), preliminary labeled with a fluorescent marker, targets, and probes match each other only if there is a perfect specific complementarity between the two sequences of those nucleotides. After a chemical wash (in order to eliminate unmatched targets still in solution), with the detection of the fluorescent signal of the hybridized targets, one can conclude on the presence—or not—of particular sequences in the patient genotype.

During static hybridization (or *cover-slip* method), where no fluid flow is applied, only molecular diffusion allows targets to move, and significant variations in the response of the chip are commonly observed, even after overnight hybridization. Indeed, by considering the diffusion coefficient of DNA in water ($D \sim 10^{-10} \text{ m}^2/\text{s}$),¹⁰ on a square chip of side $\ell \sim 1 \text{ cm}$, the typical diffusion time τ_ℓ is about

$$\tau_\ell \sim \ell^2/D \sim 300 \text{ h}, \quad (1)$$

which is absolutely incompatible with the wish to get reliable results in a reasonable time. There is thus a need to improve the reliability of the results, and speed up the process, by

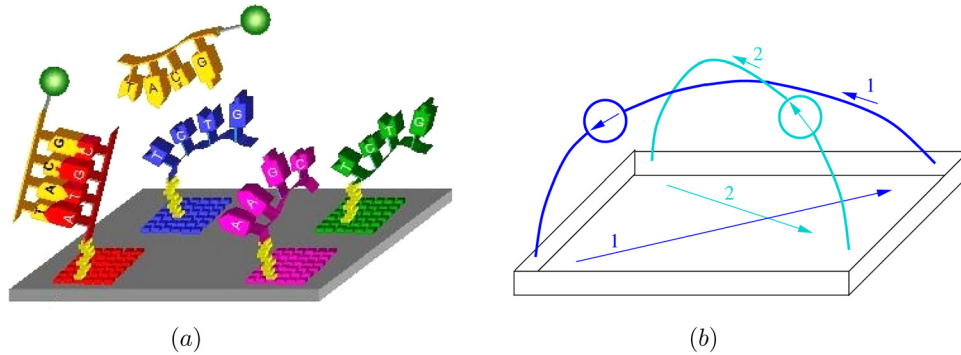


FIG. 1. (a) Schematic view of a DNA chip. The labeled free targets hybridize to their complementary probes on the chip, if present. (b) Protocol used here, which operates with two pumps switched alternately. A pump always pushes the fluid in the same direction or else is inactive.

making sure that a given target visits the whole surface of the chip in a reasonable time,^{11,12} so that hybridization can eventually take place if its complementary target is present. Since molecular diffusion alone is too slow, mixing can be achieved thanks to a flow with chaotic advection properties. In order to limit the volume, the cavity in which the chip is placed, called hybridization chamber, must have a height h as small as possible, which is exactly the configuration of Hele-Shaw cells. However, Hele-Shaw flows can, in a first approximation, be considered as two-dimensional. In those conditions, the only way to achieve chaotic advection is to make the flow non-stationary, and time-periodicity is enough.

In this article, we numerically calculate rates of reaction for systems like DNA chips, with free targets in solution and probes fixed on a surface, in a chaotic advection micromixer. The configuration chosen for the mixer is a time-periodic system with sources and sinks using pumps (Figure 1(b)), which was shown to provide efficient mixing.¹³ The hybridization chamber is rectangular of aspect ratio 3:1, therefore adapted to most DNA chips, usually manufactured on microscope lids. Indeed, using a 2D-model, we showed that the rectangular geometry enabled a more rapid and homogeneous mixing than the square geometry.¹⁴ Our goal is to compare static hybridization with hybridization in a chaotic advection micromixer.

The article is organized as follows: in a first section, we introduce the numerical model and all the parameters used in chaotic mixing; more especially, we explain *how to connect our own parameters to experimental conditions*. Then, we use our numerical results to compare static vs dynamical hybridization, in terms of typical time of decay of free targets, kinetics of reaction, and homogeneity. Finally, the last part is devoted to discuss the influence of important parameters of the model, such as molecular diffusivity of DNA strands.

II. NUMERICAL MODEL

The parameters of mixing are similar to those of our previous works on chaotic mixing:^{13,15} the hybridization chamber has a surface $S = 2.25 \text{ cm}^2$ (with sides $L = \sqrt{3S}$, $L_w = \sqrt{S/3}$), for a height $h = 50 \mu\text{m}$; the volume of the chamber is, therefore, $V_{ch} = 11.25 \mu\text{l}$, and the total volume (including pumps and tubes) is $V_{total} = 1.2 V_{ch}$. The period of the protocol of the chaotic mixer is $T = 4 \text{ s}$, and the flow rate is $q = 2 \mu\text{l/s}$.

In order to guide experimentalists on how to rely our own parameters with different experimental conditions (e.g., flow speed and chip dimensions), we remind that, as explained in a previous paper,¹⁴ the mixing problem is unchanged if the non-dimensional pulse volume

$$\alpha = \frac{qT}{hS}, \quad (2)$$

which represents the volume of fluid displaced during one period compared to the volume of the chamber, is kept constant. In this study, $\alpha \approx 0.7$, but we stress the fact that this mixing

protocol is quite robust regarding variations of α (the quality of mixing is basically unchanged if α is divided or multiplied by a factor two¹⁴). Therefore, in an experiment where the size of the chip S , the height of the chamber h , and maybe the flow-rate q imposed by the pump are given, it is always possible to adapt the period of the flow-field T so as to obtain an acceptable α ; note, however, that all time-scales (including the total time involved for the experiment) will be changed in the same proportions as T . Finally, we remind that a chemical reaction is involved in the end: it is, therefore, very important not to dilute too much the biological material and to keep the total volume (including that of external elements such as pipes and pumps) as small as experimentally possible.

A. Biological model

1. Probes

All probes are supposed to be identical, with height $\ell_p \sim 100$ nm, and are gathered on $N_s = 53$ spots of diameter $L_s \simeq 0.54$ mm, distributed as shown in Figure 2; the total surface covered by the spots is, therefore, $N_s \times \pi L_s^2/4$. A strong difficulty is to have a good estimate for the density of probes on a given spot. In practice, DNA chips can have a density varying from 10^{10} molecules per cm^2 up to as high as 10^{14} molecules per cm^2 .¹⁶ Density plays, however, a crucial role: it was shown that a too high density acted on the accessibility of the probes (sterical effects), making the hybridization more difficult and, therefore, the reaction rate lower.^{17,18} In order to get rid of any steric effect, we suppose that the distance between two adjacent probes is of the same order of magnitude as the height of the probe itself, so that there is approximately one probe for a surface ℓ_p^2 ; the density of probes is then

$$1/\ell_p^2 \approx 10^{10} \text{ probes} \cdot \text{cm}^{-2}, \quad (3)$$

which is reasonable. The total number of probes N_p on the chip is therefore

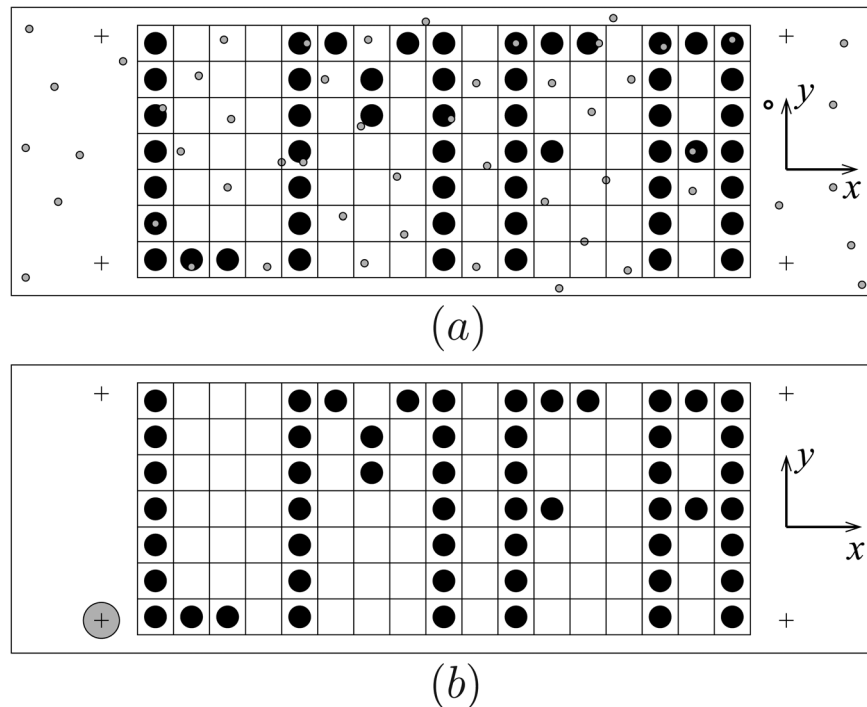


FIG. 2. Sketch of the chip: there are 53 round spots of targets. (a) Initial condition for the static hybridization. The repartition of targets is random. (b) Same for dynamic hybridization. The targets are initially located around the source on the bottom left; only their heights z are random.

$$N_p = \frac{N_s \times \pi L_s^2}{4\ell_p^2} \approx 10^9. \quad (4)$$

2. Targets

All targets are also identical and complementary to the probes. The free targets are modeled as *punctual particles* moving under the action of molecular diffusion and flow-field (the effect of size is globally included in the molecular diffusion coefficient following the Stokes-Einstein law). The initial repartition of targets has been chosen so as to follow as closely as possible the experimental conditions: in the static case, where the solution is usually mixed before being spread on the chip, the repartition is random in all three directions (Figure 2(a)). In the case of chaotic advection, the targets are initially located around a source (Figure 2(b)), and only their heights z are random, so as to model an experiment where they would be introduced using a syringe through a source. The number of initial targets N_{i0} is 40 times twice the number of spots, i.e., 2120. It is, therefore, much less than the number of probes.

3. Interaction between targets and probes

In the DNA molecule, the link between two complementary nucleotides implies hydrogen bounds, in which interactions are usually modeled using a Morse potential.¹⁹ For a piece of DNA molecule, *several* hydrogen bounds come into play, which makes the interaction between the target and the probe difficult to model.²⁰ However, our problem is slightly different here: before interacting together, the two DNA-strands have to be close enough to each other. If the targets of our model are well-mixed in the chamber, the number of targets above a spot is $N_{i0} \times \pi L_s^2 / (4S) \approx 2$, and those targets are distributed on the height h : hence a given target is generally very unlikely to be close enough to a spot so that it can feel the interaction with a probe located at the bottom of the chamber. We, therefore, use a very simple model of particle tracking, first introduced in chaotic advection for competing autocatalytical processes inside a mixing domain by Metcalfe and Ottino,²¹ which consists of a potential of infinite depth and given width d_h : hence a target is trapped (hybridized) once it comes in a d_h -vicinity of a probe (which corresponds here to a volume of height d_h above a spot of the chip). We choose the potential width d_h of the order of the size of a DNA-strand, i.e., $d_h \simeq 100 \text{ nm} \ll h$.

B. The flow field

The flow-field inside a chamber of height small compared to the other directions (a Hele-Shaw cell) has the remarkable property that the flow-field is horizontal almost everywhere and that depth-average velocity-field satisfies the Euler equation. It is, therefore, easy to obtain this quantity analytically for a source-sink inside a circle and then switch to a rectangular geometry using a Schwartz-Christoffel transformation.²² We previously used such a 2D-model in order to decide between different protocols and chamber geometries.¹⁴

However, such a 2D model where the depth-dependence of the velocity field is ignored cannot be used for our purpose: in the Hele-Shaw flow, the vertical profile is parabolic, so that the velocity vanishes on the top of the cell, but also (and more annoyingly) on the bottom where the chip is placed. This means that a target located near the bottom of the hybridization chamber will move much slower than one moving at half-depth. A depth-average flow would, therefore, favor hybridization and alter the results; this is why we reconstructed the depth parabolic dependence as follows:

- If $\bar{\mathbf{v}}(x, y, t)$ is the depth-averaged velocity vector calculated with the 2D model, then the velocity vector at point (x, y, z) and time t is given by

$$\mathbf{v}(x, y, z, t) = \frac{6\bar{\mathbf{v}}(x, y, t)}{h^2} z(h - z). \quad (5)$$

- When a fluid particle is swallowed into a sink, it is swallowed up with a random depth, the density probability function of which follows a parabolic rule.

As a validation, we compared the results obtained with this model with those of complete 3D calculations of the Stokes equation in a *square* geometry, with a chaotic mixing protocol previously studied (see details in Ref. 15): in Figure 3 are shown two Poincaré sections for the same case of rather bad mixing, where a large regular region (region empty of points or with closed curves) is clearly visible, obtained by the complete 3D calculations or by our 3D model. The similarity between both is excellent.

C. Molecular diffusion and trajectories

The total displacement of a given target is thus obtained using

$$\frac{d\mathbf{x}}{dt} = \mathbf{v}(x, y, z, t) + \zeta(t), \quad (6)$$

where $\mathbf{x}(t)$ is the particle position at time t , $\mathbf{v}(x, y, z, t)$ is the 3D-modeled velocity field; $\zeta(t)$ models the molecular diffusion and is a Gaussian decorrelated process such that $\langle \zeta_i(t) \zeta_j(t') \rangle = 2D \delta_{ij} \delta(t - t')$, where D is the diffusion coefficient, δ_{ij} is the Kronecker symbol ($\delta_{ij} = 1$ if $i = j$, zero otherwise), and δ is the Dirac delta function. The trajectories are integrated using a fourth-order Runge-Kutta method. Note that in the static case (no flow-field), $\mathbf{v}(x, y, z, t) = \mathbf{0}$.

III. COMPARISON STATIC/DYNAMICAL HYBRIDIZATION

In the following, the diffusion coefficient D of the free targets is taken equal to $10^{-10} \text{ m}^2 \text{ s}^{-1}$.

A. Decay of free targets

Figure 4 shows in log-lin plot the decay of free targets as a function of time, with or without chaotic advection. We observe that the hybridization is much faster in the dynamical case. Moreover, the decay is exponential with chaotic advection, as generally expected for a chemical reaction with perfect mixing, whereas it is not exponential at short times in the static case (but the exponential behavior is recovered at large times). We find that the hybridization is about 100 times more rapid with dynamical hybridization compared to the static case.

B. Kinetics of reaction

The kinetics of reaction is usually measured experimentally in the static case. From our model, we want to recover the order of magnitude of the rate of reaction, assuming that the

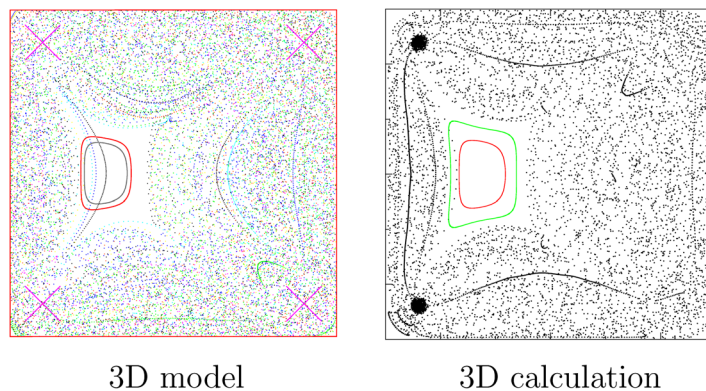


FIG. 3. Comparison of two Poincaré sections (the successive positions of given particles taken at each period is accumulated on the section) of the same protocol¹⁵ with the same period $T = 4 \text{ s}$ in a square chamber. The left one is calculated with the 3D model, while the right one results from a complete 3D calculation.

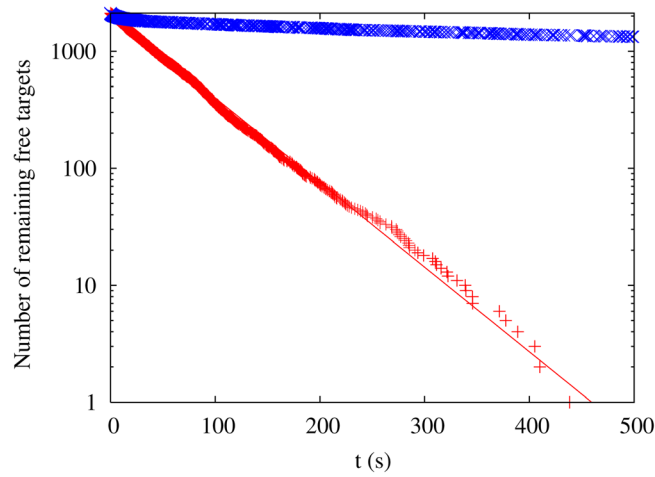


FIG. 4. Decay of free targets as a function of time; blue \times : static case; red $+$: with chaotic advection. The diffusion coefficient is in both cases $D = 10^{-10} \text{ m}^2 \text{ s}^{-1}$. The straight line in log-lin scale indicates that the decay is of the type $\exp(-t/\tau)$.

limiting process is the time needed for a given target to approach a probe. The reaction between a target and a probe can generally be written as



where T stands for free target, P for free probe, and TP for the hybridized strand; k_a is the reaction rate constant for hybridization, and k_d is the analogue for the opposite. In the well mixed problem, where the concentrations of all species are uniform and equal to the mean concentrations, we have^{23–26}

$$-\frac{d[T]}{dt} = -\frac{d[P]}{dt} = \frac{d[TP]}{dt} = k_a[T][P] - k_d[TP], \quad (8)$$

where $[A]$ stands for the concentration of species A , and we denote by $[A]_0$ the concentration of A at time $t=0$. Because of the large number of hydrogen bonds involved in the DNA strand, the deshybridization reaction is very unlikely at temperatures involved in DNA-chips, so that we consider that $k_d = 0$. We can, therefore, solve Eq. (8), and in the case of excess of probes ($[P]_0 \gg [T]_0$), $[P]$ can be considered as constant ($[P] \approx [P]_0$), and we obtain

$$[T] = [T]_0 \exp(-t k_a [P]_0). \quad (9)$$

We recover an exponential decay as in our numerical simulations. Therefore, from the slope τ of Figure 4, we obtain the constant k_a

$$k_a = \frac{1}{\tau \times [P]_0}. \quad (10)$$

The initial volumic concentration in probes, expressed in moles per liters is

$$[P]_0 = \frac{N_P}{\mathcal{N}_a \times S \times h}, \quad (11)$$

where \mathcal{N}_a is the Avogadro number. Taking $\mathcal{N}_a = 6.02 \times 10^{23}$, $S = 2.25 \text{ cm}^2$, $h = 50 \text{ }\mu\text{m}$, we obtain a reasonable value for $[P]_0$

$$[P]_0 = 1.79 \times 10^{-10} \text{ mol. l}^{-1}. \quad (12)$$

From Eq. (10), we obtain k_a both in the static and dynamical case

$$k_a^{\text{stat}} \approx 10^6 \text{ M}^{-1} \text{ s}^{-1} \quad (13)$$

and

$$k_a^{\text{dyn}} \approx 10^8 \text{ M}^{-1} \text{ s}^{-1}, \quad (14)$$

where M is the usual symbol for mol.l^{-1} . Those results are all the more interesting that, with our very simple model, we recover the same order of magnitude for k_a in the static case as the one found experimentally by various authors!^{24–26} This suggests that diffusion is the limiting process in most experiments of this kind.

C. Homogeneity

The homogeneity of hybridization is also an important criterion in those technologies where a “large” surface is considered: the probability to end on any spot must be as uniform as possible. Therefore, we introduce an instantaneous non-dimensional standard deviation defined as

$$\sigma(t) = \frac{1}{N_t^h(t)} \sqrt{\sum_{i=1}^{N_s} \left(N_{t,i}^h(t) - \frac{N_t^h(t)}{N_s} \right)^2}, \quad (15)$$

where $N_t^h(t)$ is the total number of hybridized targets at time t , while $N_{t,i}^h(t)$ is the number of hybridized targets on spot i . Those two quantities are linked by the relation

$$N_t^h(t) = \sum_{i=1}^{N_s} N_{t,i}^h(t). \quad (16)$$

The variance in Eq. (15) is renormalized at all times by the number of hybridized targets $N_t^h(t)$. If all targets are hybridized on the same spot (the worst case),

$$\sum_{i=1}^{N_s} \left(N_{t,i}^h(t) - \frac{N_t^h(t)}{N_s} \right)^2 = \left(N_t^h(t) - \frac{N_t^h(t)}{N_s} \right)^2 + (N_s - 1) \left(\frac{N_t^h(t)}{N_s} \right)^2, \quad (17)$$

$$= (N_t^h)^2 \left(1 - \frac{1}{N_s} \right), \quad (18)$$

and finally $\sigma(t) = (1 - 1/N_s)^{1/2} \approx 1$. In case of perfect homogeneity ($\forall i, N_{t,i}^h(t) = N_t^h(t)/N_s$), one obtains zero. Therefore, σ is between 0 (perfect homogeneity) and 1 (bad homogeneity). As can be seen in Figure 5 in log-log scale, although static hybridization is more homogeneous at very short times, which can be explained by the fact that targets are initially well-mixed in that case, dynamical hybridization becomes more homogeneous after only 2 periods of the flow-field (i.e., 8 s). Those results are in accordance with the experiment performed in a prototype mixer, where we showed that chaotic advection improved not only the rapidity but also the homogeneity and selectivity of hybridization.²⁷

IV. GENERALIZATION: INFLUENCE OF d_h AND D

From our theoretical results above and the experimental results, we suspect that the limiting process for the reaction is the time taken by the target to approach the probe “close enough” so that chemical interactions come into play. In our model, however, we supposed, quite arbitrarily, that the distance of interaction was $d_h = 100 \text{ nm}$. How would the previous results depend

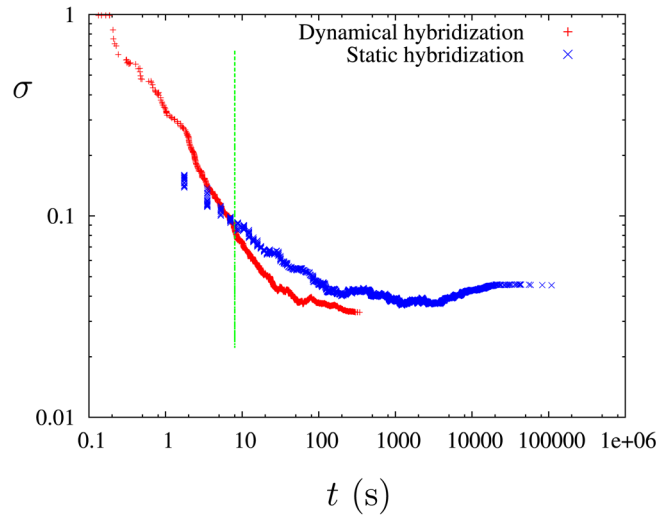


FIG. 5. Homogeneity of hybridization; blue \times : static case; red $+$: with chaotic advection. The green line corresponds to 2 periods of the flow-field. The diffusion coefficient is in both cases $D = 10^{-10} \text{ m}^2 \text{ s}^{-1}$.

on that parameter? Moreover, since mixing depends on the diffusion coefficient (all the more in the static case where diffusion is the limiting process), what happens when the diffusion coefficient is varied? We performed many such different numerical experiments, with d_h varying from 25 nm up to $50 \text{ }\mu\text{m}$ (the height of the chamber!) and three different values of D from $10^{-10} \text{ m}^2 \text{ s}^{-1}$ up to $10^{-12} \text{ m}^2 \text{ s}^{-1}$.

A. Static case

Figure 6(a) shows the typical times in the static case (no flow). The results are striking: when only diffusion can move the targets, *the rate of decay of free targets does absolutely not depend on d_h* ! This can be easily explained: on the one hand, the characteristic diffusion time in the vertical direction is, from Eq. (1) with $D = 10^{-10} \text{ m}^2/\text{s}$ and height $\ell = h = 50 \text{ }\mu\text{m}$, of the order of 25 s; on the other hand, the typical horizontal distance between two targets in the well-mixed case is $\sqrt{S/N_{t0}} \simeq 300 \text{ }\mu\text{m}$, which corresponds to a typical horizontal diffusion time 900 s (and even higher if the targets are not initially well-mixed). Therefore, the limiting process in the static case is the horizontal displacement, and we can make the rate of decay

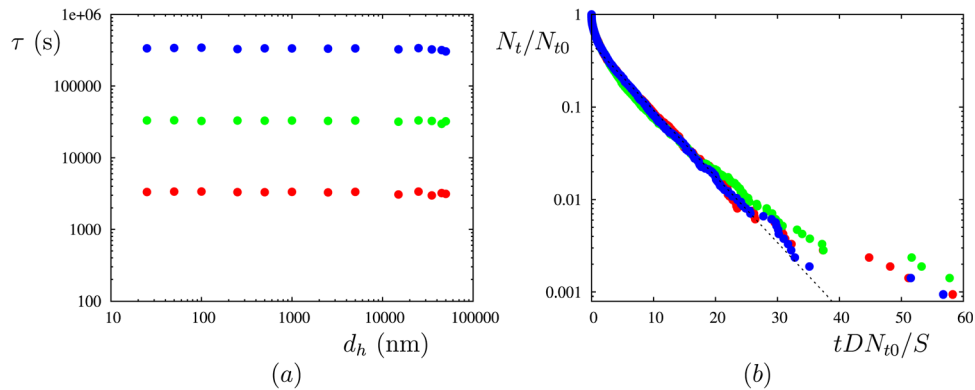


FIG. 6. (a) Typical time of decay of free target τ (log-log plot) in the static case as a function of d_h for different values of D . Red symbols: $D = 10^{-10} \text{ m}^2 \text{ s}^{-1}$; green symbols: $D = 10^{-11} \text{ m}^2 \text{ s}^{-1}$; blue symbols: $D = 10^{-12} \text{ m}^2 \text{ s}^{-1}$; (b) decay of free targets for the same values of D (log-lin plot) as a function of the non-dimensional time tDN_{t0}/S (which takes into account the initial distance between two free targets) for $d_h = 100 \text{ nm}$: the three curves collapse.

non-dimensional using the typical time $S/(N_{i0}D)$, as shown in Figure 6(b): the rate of decay is directly proportional to D^{-1} , following a diffusion process.

B. Dynamical case (with chaotic mixing)

Figure 7 shows the time of decay τ in the chaotic mixing case. Once again, when considering only physically reasonable values of d_h , from 25 nm up to 500 nm, *the time of decay of free targets still does not depend on d_h* , although, for even larger values of d_h (1000 nm and higher), as expected, targets hybridize more rapidly.

However, τ is shown to depend strongly on D . We remind that mixing is characterized by the Péclet number

$$Pe = \frac{q}{hD}, \quad (19)$$

which measures the relative time scales of displacement by the flow-field ($L/U = LL_w h/q$, where U is the typical velocity) with that of diffusion (S/D , where $S = LL_w$). Here, the Péclet number varies from $4 \cdot 10^5$ up to $4 \cdot 10^7$. Therefore, using the Buckingham π theorem, we expect τ to behave like

$$\tau \approx \frac{L}{U} f(Pe), \quad (20)$$

$$\approx \frac{Sh}{q} f(Pe), \quad (21)$$

where f is a function to determine. Dealing with chaotic advection, we would expect f to display a very weak dependence in Pe , typically like $\log(Pe)$.²⁸ This is obviously not the case here. In order to explain why, and find the correct expression for f , we will try to understand how the targets enter a volume of hybridization, as sketched on Figure 8: on the one hand, the velocity field near the bottom is very weak and cannot explain the renewing of targets in the interaction region (we recall that the flow-field is horizontal almost everywhere in a Hele-Shaw flow, so that we can neglect vertical advection); on the other hand, the volume of hybridization is very small in height, so that the typical renewing time of fluid inside the volume is governed by the vertical diffusion, d_h^2/D , which, with $d_h = 100$ nm and $D = 10^{-10} \text{ m}^2 \text{ s}^{-1}$, is even smaller than a millisecond (typical horizontal diffusion time is L_s^2/D , which makes horizontal diffusion

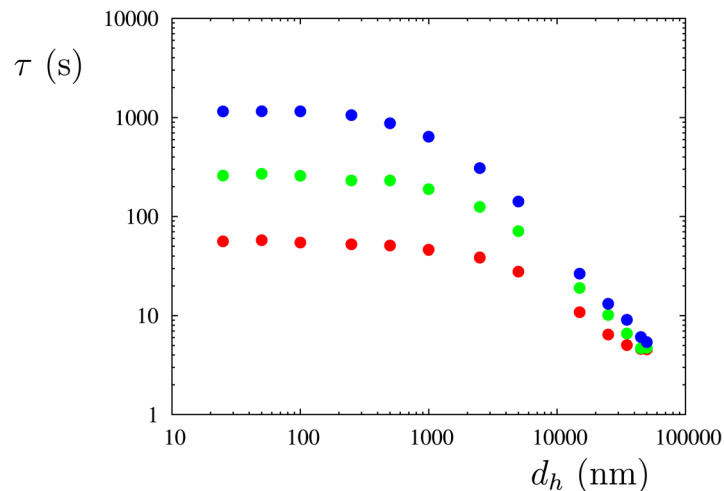


FIG. 7. Typical time of decay of free target τ (log-log plot) in the dynamical case as a function of d_h for different values of D . Red symbols: $D = 10^{-10} \text{ m}^2 \text{ s}^{-1}$; green symbols: $D = 10^{-11} \text{ m}^2 \text{ s}^{-1}$; blue symbols: $D = 10^{-12} \text{ m}^2 \text{ s}^{-1}$.

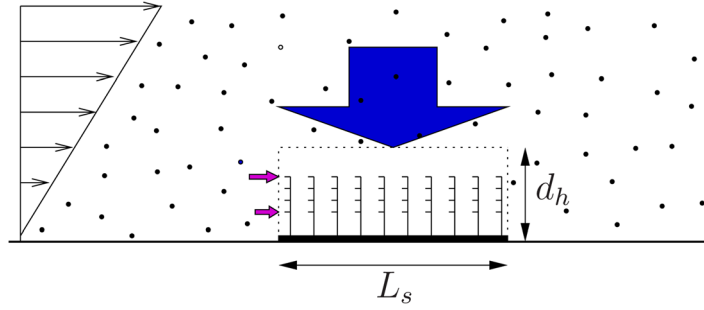


FIG. 8. Typical mechanisms of renewing of fluid inside the hybridization volume: advection is very weak near the bottom, while the very small height of the volume allows a good vertical exchange of fluid by molecular diffusion.

more than 10^7 less efficient than vertical diffusion)! Therefore, we must understand how fresh fluid is brought above the spot. For this, we suppose that at a given time t , there are no more targets above a spot (Figure 9). On one hand, the typical advection time to bring targets above the spot at height z is $L_s/v(z)$. Since $v(z)$ is an increasing function of z up to mid-height, the corresponding time-scale is a decreasing function of z , and the advection mechanism is more efficient when z is increased. On the other hand, the typical diffusion time at height z is z^2/D , which is an increasing function of z . Therefore, the physically efficient value of z is d_h^{eff} , height at which the two time-scales are equal, such that as much fresh fluid is brought above the spot as the quantity that mixes vertically, and we have

$$\frac{L_s}{v(d_h^{eff})} = \frac{d_h^{eff2}}{D}, \quad (22)$$

where the parabolic profile in z (Eq. (5)) for small z implies

$$v(d_h^{eff}) \approx \frac{6 d_h^{eff}}{h} \frac{q}{h L_w}. \quad (23)$$

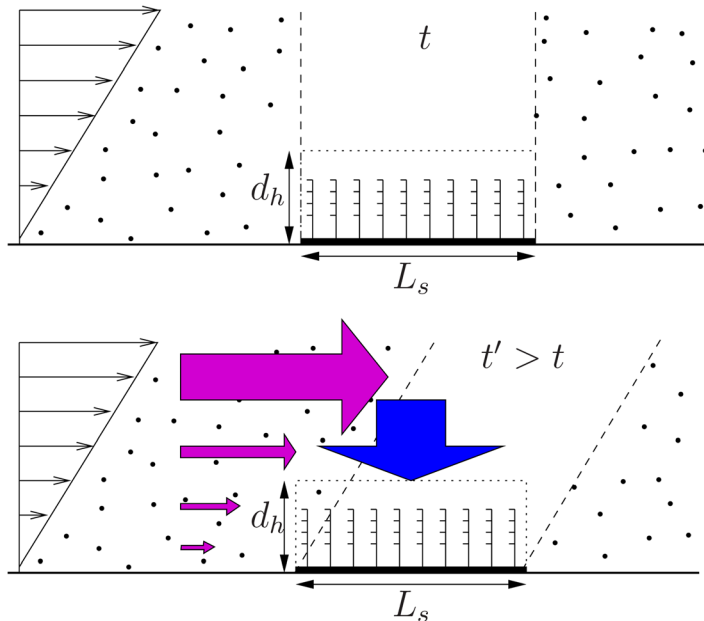


FIG. 9. Top: at a given time t , we suppose that there are no more targets above a spot. At a time $t' > t$, when considering the sole action of advection, some targets have been moved above the spot by the velocity field; they can be brought back inside the hybridization volume by molecular diffusion.

We, therefore, obtain

$$d_h^{eff3} = \frac{L_s h L_w}{6 Pe}, \quad (24)$$

and finally

$$d_h^{eff} = d_{h,0}^{eff} Pe^{-1/3}, \quad (25)$$

with

$$d_{h,0}^{eff} = \left(\frac{L_s h L_w}{6} \right)^{1/3}. \quad (26)$$

Since we have an exponential decrease of the number of free targets N_t , we can write

$$-\frac{1}{N_t} \frac{dN_t}{dt} = \frac{1}{\tau} = \frac{1}{\tau^{eff}} \frac{V^{eff}}{V_{total}}, \quad (27)$$

where $\tau^{eff} = d_h^{eff2}/D$ is the characteristic time of renewing of fluid above a spot, and V^{eff} is the corresponding effective volume above *all* spots, i.e., $V^{eff} = N_s d_h^{eff} \pi L_s^2/4$. From Eqs. (24) and (27), we get

$$\tau \approx \frac{d_h^{eff2}}{D} \frac{4 \times 1.2 L L_w h}{N_s \pi L_s^2 d_h^{eff}}, \quad (28)$$

$$\approx d_h^{eff} \frac{q}{hD} \frac{8.4 L L_w h^2}{N_s \pi L_s^2 q}, \quad (29)$$

$$\approx \tau_0 Pe^{2/3}, \quad (30)$$

with

$$\tau_0 = \frac{8.4 h^{7/3} L_w^{4/3} L}{6^{1/3} N_s \pi L_s^{5/3} q}. \quad (31)$$

Therefore, using Eqs. (25) and (30), Figure 7 can be plotted using $\tau/\tau_0 Pe^{-2/3}$ as a function of $d_h/d_{h,0}^{eff} Pe^{1/3}$. This is done in Figure 10: in the horizontal scale, the plateau extends up to values of $d_h/d_{h,0}^{eff} Pe^{1/3}$ of order 1, while it corresponds roughly to a value of 1 in the vertical scale $d_h/d_{h,0}^{eff} Pe^{1/3}$. This is in accordance with the mechanism presented above, and, because fresh fluid is brought in the interaction zone by vertical diffusion in the end, the function f in Eq. (21) is an algebraic function and not a logarithm function. This explains why d_h plays no role in the result, in accordance with the idea that the detailed structure of the interaction potential plays little role in the particle dynamics. This also explains why the gain in hybridization velocity when comparing static and dynamical hybridizations is lower than the gain found in mixing time with our 2D model (mixing about 1000 times more rapid in the dynamical case,¹⁴ while we have a factor 100 “only” here): although the horizontal dispersion is 1000 times more rapid at mid-height, the fresh fluid is brought to the bottom by molecular diffusion only.

We also checked the dependence of τ in L_s (diameter of the spots). This is done in Figure 11 in the case $D = 10^{-10} \text{ m}^2 \text{ s}^{-1}$ and $d_h = 100 \text{ nm}$: clearly, τ depends on $L_s^{-5/3}$, as found in Eq. (31), which is very important in practice concerning this technology.

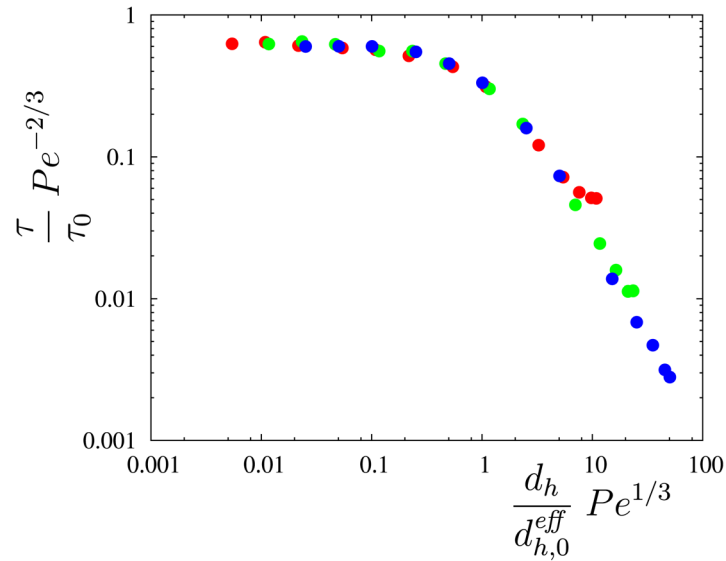


FIG. 10. Non-dimensional τ (log-log plot) in the dynamical case using Eq. (30) as a function of non-dimensional d_h using Eq. (25) for different values of D from $10^{-10} \text{ m}^2 \text{ s}^{-1}$ up to $10^{-12} \text{ m}^2 \text{ s}^{-1}$ (same as in Fig. 7). The values of $d_{h,0}^{eff}$ and τ_0 are given, respectively, in Eqs. (26) and (31). The three sets of points collapse on the same curve.

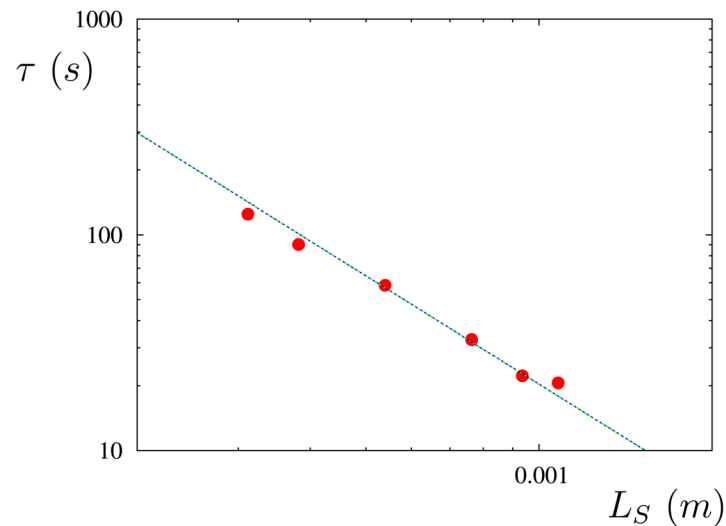


FIG. 11. τ (log-log plot) in the dynamical case as a function of the diameter of the spots L_S ; the fit is a power law with slope $-5/3$.

V. CONCLUSIONS

In this paper, we numerically compared static hybridization with hybridization when chaotic advection is involved. The flow-field is a periodic flow in a rectangular chamber of small height. Our numerical model is very simple: the targets are supposed to be passive scalars that move inside the hybridization chamber thanks to the velocity field and molecular diffusion. The hybridization occurs as soon as a target comes inside a hybridization volume of height d_h above a spot of probes (capture model). The velocity field is reconstructed in volume starting from a 2D model that enables to find it analytically, which makes it easier to integrate and follow the targets.

We checked numerically and explained why the exact knowledge of the details of interaction (here the distance of interaction d_h) plays almost no role in the results. We also showed

that with our model, hybridization is about 100 times more rapid than the usual static hybridization, in accordance with our previous experimental results. We then estimated the kinetics of reaction: our numerical results in the static case are in total agreement with the experimental results in the literature, suggesting that most authors calculate the time needed by the target to approach the probe under the sole action of molecular diffusion, rather than the reaction rate itself. We, therefore, suggest that the kinetics of reaction should always be measured experimentally in a dynamical case, rather than using static hybridization, as done until now.

Moreover, we show that even when chaotic advection is involved, targets are brought inside the hybridization volume thanks to molecular diffusion in the end, which explains why we observe an algebraic (rather than logarithmic) dependence on the Péclet number. We explain theoretically this dependence, together with the fact that the value of d_h plays no crucial role in our model.

ACKNOWLEDGMENTS

We thank Jean-Pierre Cloarec for discussions on a plausible value of d_h and Jean-Noël Gence for his help in density probability functions for the parabolic profile for targets reinjection.

- ¹H. A. Stone, A. D. Stroock, and A. Ajdari, "Engineering flows in small devices: Microfluidics toward lab-on-a-chip," *Annu. Rev. Fluid Mech.* **36**, 381–411 (2004).
- ²H. Aref, "Stirring by chaotic advection," *J. Fluid Mech.* **143**, 1–21 (1984).
- ³S. Wiggins, *Global Bifurcations and Chaos* (Springer-Verlag, 1988).
- ⁴J. M. Ottino, *The Kinematics of Mixing: Stretching, Chaos and Transport* (Cambridge University Press, New York, 1989).
- ⁵V. Toussaint, Ph. Carrière, and F. Raynal, "A numerical Eulerian approach to mixing by chaotic advection," *Phys. Fluids* **7**, 2587–2600 (1995).
- ⁶A. D. Stroock, S. K. W. Dertinger, A. Ajdari, I. Mezic, H. A. Stone, and G. M. Whitesides, "Chaotic mixer for microchannels," *Science* **295**, 647–651 (2002).
- ⁷S. Cerbelli, V. Vitacolonna, A. Adrover, and M. Giona, "Eigenvalue–eigenfunction analysis of infinitely fast reactions and micromixing regimes in regular and chaotic bounded flows," *Chem. Eng. Sci.* **59**, 2125–2144 (2004).
- ⁸S. Cerbelli, F. Garofalo, and M. Giona, "Steady-state performance of an infinitely fast reaction in a three-dimensional open Stokes flow," *Chem. Eng. Sci.* **63**(17), 4396–4411 (2008).
- ⁹R. T. Pon and S. Yu, "Linker phosphoramidite reagents for the attachment of the first nucleoside to underivatized solid-phase supports," *Nucleic Acids Res.* **32**, 623–631 (2004).
- ¹⁰A. E. Nkodo, J. M. Garnier, B. Tinland, H. Ren, C. Desruisseaux, L. C. McCormick, G. Drouin, and G. W. Slater, "Diffusion coefficient of DNA molecules during free solution electrophoresis," *Electrophoresis* **22**(12), 2424–2432 (2001).
- ¹¹C. J. Schaupp, G. Jiang, T. G. Myers, and M. A. Wilson, "Active mixing during hybridization improves the accuracy and reproducibility of microarray results," *BioTechniques* **38**(1), 117–119 (2005).
- ¹²O. Y. F. Henry and C. K. O. Sullivan, "Rapid DNA hybridization in microfluidics," *TrAC, Trends Anal. Chem.* **33**(0), 9–22 (2012).
- ¹³F. Raynal, A. Beuf, F. Plaza, J. Scott, P. Carriere, M. Cabrera, J.-P. Cloarec, and E. Souteyrand, "Towards better DNA chip hybridization using chaotic advection," *Phys. Fluids* **19**(1), 017112 (2007).
- ¹⁴A. Beuf, J.-N. Gence, Ph. Carrière, and F. Raynal, "Chaotic mixing efficiency in different geometries of Hele-Shaw cells," *Int. J. Heat Mass Transfer* **53**(4), 684–693 (2010).
- ¹⁵F. Raynal, F. Plaza, A. Beuf, Ph. Carrière, E. Souteyrand, J.-R. Martin, J.-P. Cloarec, and M. Cabrera, "Study of a chaotic mixing system for DNA chip hybridization chambers," *Phys. Fluids* **16**(9), L63–L66 (2004).
- ¹⁶J.-P. Cloarec, Y. Chevolut, E. Laurenceau, M. Phaner-Goutorbe, and E. Souteyrand, "A multidisciplinary approach for molecular diagnostics based on biosensors and microarrays," *IRBM News* **29**(23), 105–127 (2008).
- ¹⁷V. Chan, D. J. Graves, and S. E. McKenzie, "The biophysics of DNA hybridization with immobilized oligonucleotide probes," *Biophys. J.* **69**, 2243–2255 (1995).
- ¹⁸M. R. Henry, "Real-time measurements of DNA hybridization on microparticles with fluorescence resonance energy transfer," *Anal. Biochem.* **276**, 204–214 (1999).
- ¹⁹T. Dauxois, M. Peyrard, and A. R. Bishop, "Dynamics and thermodynamics of a nonlinear model for DNA denaturation," *Phys. Rev. E* **47**(1), 684–695 (1993).
- ²⁰M. Peyrard, S. Cuesta-López, and G. James, "Modelling DNA at the mesoscale: A challenge for nonlinear science?," *Nonlinearity* **21**(6), T91 (2008).
- ²¹G. Metcalfe and J. M. Ottino, "Autocatalytic processes in mixing flows," *Phys. Rev. Lett.* **72**(18), 2875–2878 (1994).
- ²²L. M. Milne-Thomson, *Theoretical Hydrodynamics*, 5th ed. (Macmillan, 1968).
- ²³D. Erickson, D. Li, and J. Krull, "Modelling of DNA hybridization kinetics for spatially resolved biochips," *Anal. Biochem.* **317**(2), 186–200 (2003).
- ²⁴H.-P. Lehr, M. Reimann, A. Brandenburg, G. Sulz, and H. Klapproth, "Real-time detection of nucleic acid interactions by total internal reflection fluorescence," *Anal. Chem.* **75**(10), 2414–2420 (2003).
- ²⁵J. Zeng, A. Almadidy, J. Watterson, and U. J. Krull, "Interfacial hybridization kinetics of oligonucleotides immobilized onto fused silica surfaces," *Sens. Actuators B* **90**, 68–75 (2003).

- ²⁶Y. Zhang, D. A. Hammer, and D. J. Graves, "Competitive hybridization kinetics reveals unexpected behavior patterns," *Biophys. J.* **89**, 2950–2959 (2005).
- ²⁷F. Raynal, A. Beuf, F. Plaza, P. Carrière, M. Cabrera, J.-P. Cloarec, V. Dugas, E. Fradier, and É. Souteyrand, "Chaotic mixing in a Hele-Shaw cell, with applications to DNA chip hybridization," in *The Proceedings of MicroTAS 2007 Conference*, 307 Laurel Street, San Diego, California 92101-1630, USA, edited by J.-L. Viovy, P. Tabeling, S. Descroix, and L. Malaquin (Chemical and Biological Microsystems Society, 307 Laurel Street, San Diego, CA 92101-1630, 2007), pp. 901–903.
- ²⁸F. Raynal and J. N. Gence, "Energy saving in chaotic laminar mixing," *Int. J. Heat Mass Transfer* **40**(14), 3267–3273 (1997).